Highly Integrated Workflows for Exploring Cardiovascular Conditions: Exemplars of Precision Medicine in Alzheimer's Disease and Aortic Dissection

John C. VARDAKIS[1,*], Mirko BONFANTI[1,2,*], Gaia FRANZETTI[1], Liwei GUO[1], Toni LASSILA[3], Micaela MITOLO[5], Milton HOZ DE VILA[3], John P. GREENWOOD[7,8], Gabriele MARITATI[9,10], Dean CHOU[12], Zeike A. TAYLOR[4], Annalena VENNERI[6], Shervanthi HOMER-VANNIASINKAM[1,8,11], Stavroula BALABANI[1], Alejandro F. FRANGI[3], Yiannis VENTIKOS[1] & Vanessa DIAZ-ZUCCARINI[1,2]

*[1]Department of Mechanical Engineering, University College London, Torrington Place, London, WC1E 7JE, UK, *email: {v.diaz, y.ventikos}@ucl.ac.uk*

[2]Wellcome/EPSRC Centre for Interventional and Surgical Sciences (WEISS), Department of Medical Physics and Biomedical Engineering, University College London, UK

[3]Centre for Computational Imaging & Simulation Technologies in Biomedicine (CISTIB), School of Computing, University of Leeds, UK

[4]Centre for Computational Imaging & Simulation Technologies in Biomedicine (CISTIB), School of Mechanical Engineering, University of Leeds, UK

[5]Functional MR Unit, Policlinico S. Orsola e Malpighi, Department of Biomedical and NeuroMotor Sciences (DiBiNeM), Bologna, Italy.

[6]Department of Neuroscience, Medical School, University of Sheffield, UK.

[7]Leeds Institute of Cardiovascular and Metabolic Medicine, University of Leeds, UK

[8]Leeds Teaching Hospitals NHS Trust, Leeds, UK

[9]Ospedale A. Perrino, Brindisi, Italy

[10]Azienda Ospedaliera San Camillo-Forlanini, Rome, Italy

[11]University of Warwick Medical School & University Hospitals Coventry and Warwickshire NHS Trust, Coventry, UK.

[12]Department of Mechanical Engineering, National Central University, Taoyuan County, Taiwan

* The first two authors contributed equally to this study

Key words: Alzheimer's Disease, Aortic Dissection, Computational Fluid Dynamics, Dementia, Glymphatic system, Haemodynamics, Multiple-Network Poroelastic Theory, Virtual Physiological Human (VPH)

Abstract

For precision medicine to be implemented through the lens of *in silico* technology, it is imperative that biophysical research workflows offer insight into treatments that are specific to a particular illness and to a particular subject. The boundaries of precision medicine can be extended using multiscale, biophysics-centred workflows that consider the fundamental underpinnings of the constituents of cells and tissues and their dynamic environments. Utilising numerical techniques that can capture the broad spectrum of biological flows within complex, deformable and permeable organs and tissues is of paramount importance when considering the core prerequisites of any state-of-the-art precision medicine pipeline. In this work, a succinct breakdown of two precision medicine pipelines developed within two Virtual Physiological Human (VPH) projects are given. The first workflow is targeted on the trajectory of Alzheimer's Disease, and caters for novel hypothesis testing through a multicompartmental poroelastic model which is integrated with a high throughput imaging workflow and subject-specific blood flow variability model. The second workflow gives rise to the patient specific exploration of Aortic Dissections via a multi-scale and compliant model, harnessing imaging, computational fluid-dynamics (CFD) and dynamic boundary conditions. Results relating to the first workflow include some core outputs of the multiporoelastic modelling framework, and the representation of peri-arterial swelling and peri-venous drainage solution fields. The latter solution fields were statistically analysed for a cohort of thirty-five subjects (stratified with respect to disease status, gender and activity level). The second workflow allowed for a better understanding of complex

aortic dissection cases utilising both a rigid-wall model informed by minimal and clinically common datasets as well as a moving-wall model informed by rich datasets.

Mots clés : Maladie d'Alzheimer, Dissection aortique, Dynamique des fluides computationnelle, Démence, Système lymphatique, Hémodynamique, Théorie poroélastique à réseaux multiples, Physiologie humaine virtuelle (VPH)

Résumé
Pour que la médecine actuelle puisse profiter de la technologie in silico, il est impératif que les flux de recherche biophysique offrent un aperçu précis des traitements spécifiques à une maladie particulière et à un sujet particulier. Les limites de la médecine peuvent être repoussées à l'aide de flux de travail multi-échelles, centrés sur la biophysique, qui tiennent compte des constituants fondamentaux des cellules et des tissus, et de leurs environnements dynamiques. L'utilisation de techniques numériques permettant de capter le large spectre des flux biologiques au sein d'organes et de tissus complexes, déformables et perméables est d'une importance capitale lorsqu'il s'agit d'examiner les conditions essentielles de tout pipeline médical de précision de pointe. Dans ce travail, une brève ventilation de deux pipelines de médecine de précision développés dans le cadre de deux projets VPH (Virtual Physiological Human) est donnée. Le premier flux de travail se concentre sur la trajectoire de la maladie d'Alzheimer et permet de tester de nouvelles hypothèses au moyen d'un modèle poroélastique à plusieurs compartiments qui est intégré à un flux de travail d'imagerie à haut débit et à un modèle de variabilité du débit sanguin spécifique au sujet. Le deuxième flux de travail donne lieu à l'exploration spécifique au patient des dissections aortiques par le biais d'un modèle multi-échelle et conforme, exploitant l'imagerie, la dynamique des fluides computationnelle (CFD) et les conditions limites dynamiques. Les résultats relatifs au premier flux de travail comprennent certains des principaux extrants du cadre de modélisation multiporoélastique et la représentation des champs de gonflement péri-artériel et de solution de drainage périveineux. Ces derniers champs de solutions ont été analysés statistiquement pour une cohorte de trente-cinq sujets (stratifiés en fonction de l'état pathologique, du sexe et du niveau d'activité). Le deuxième flux de travail a permis de mieux comprendre les cas complexes de dissection aortique à l'aide d'un modèle à parois rigides fondé sur des ensembles de données minimales et cliniquement communes et d'un modèle à parois mobiles fondé sur de ensembles de données riches.

1. INTRODUCTION

For precision medicine to be implemented within the paradigm of in silico technology, it is imperative that biophysical research workflows offer insight into treatments that are both disease and subject-specific. The boundaries of precision medicine can be extended using such multiscale workflows, but it is imperative that they are able to consider the fundamental underpinnings of the constituents of cells and tissues and their dynamic environments. A secondary motivation to this work is also the rising ethical concerns surrounding animal experimentation which is cultivating growing interest in alternative methods, such as *in vitro* or *in silico* technologies [1]. The utilisation of numerical techniques that can capture the broad spectrum of biological flows within complex three-dimensional, deformable and permeable organs and tissues is of paramount importance when considering the core prerequisites of any state-of-the-art precision medicine pipeline. In this manuscript, two pipelines that were developed within two VPH projects are described, namely VPH-Dementia Research Enabled by IT (VPH-DARE@IT, www.vph-dare.eu) and VPH-Cardiovascular Simulation and Experimentation for Personalised Medical Devices (VPH-CaSE, www.vph-case.eu). Within VPH-DARE@IT, one of the core objectives of the project was to extend the understanding of dementia (with a focus on the trajectory of Alzheimer's Disease through novel hypothesis testing) in addition to promoting earlier differential diagnosis through a unified multi-scale modelling approach (revolving around a multicompartmental

poroelastic model) that fully accounts for environmental influences on biophysics, physiology, novel clinical biomarkers and lifestyle. VPH-CaSE focused on cardiovascular medical devices and offered a highly integrated knowledge-exchange pipeline revolving around cardiac tissue function and cardiac support, cardiovascular haemodynamics and image-based diagnosis and imaging quality assurance. Through this pipeline, patient specific explorations of Aortic Dissections were performed, via a multi-scale and compliant model, harnessing imaging, CFD and dynamic boundary conditions.

1.1 Alzheimer's Disease (AD) and the Glymphatic system

The global cost of dementia is expected to reach $2 trillion by 2030. By 2050, it is estimated that over 150 million people will be living with dementia [2]. Alzheimer's Disease (AD) accounts for approximately 70% of all dementia cases [3], and is characterized by a heterogeneous mixture of multiple age-related neurodegenerative factors and vascular related pathologies. The hallmark pathological features of the disease are the extracellular deposition of amyloid-β (Aβ) peptide into parenchymal senile plaques or within the walls of arteries and capillaries, in addition to the aggregation of hyperphosphorylated tau into intracellular neurofibrillary tangles and neuropil threads [4,5]. Evidence suggests that AD may be a vascular disorder [6,7], caused by impaired cerebral perfusion (characterized by reduction in both total and regional cerebral blood flow (CBF) [8]) [7,9], which is observable at the prodromal stages of the disease [10,12]. Hypoperfusion can compromise the oxygenation of neurons, negatively affect the synthesis of proteins required for memory and learning and subsequently lead to neuronal dysfunction or death [13,14]. During this early stage of the disease, AD may present itself as mild cognitive impairment (MCI), an intermediate state between normal ageing and dementia. Traditionally, MCI has been defined as a condition whereby an individual experiences memory loss to a greater extent than that expected for that age but does not meet the criteria for dementia [16]. Clearance of Aβ at the level of the blood–brain barrier (BBB), an important part of the neurovascular unit (NVU), is also important in preventing plaque accumulation [15].

The interstitial fluid (ISF) of the brain is tasked with providing the environment for healthy neuronal functioning. It is therefore vital that the maintenance of the ISFs volume and composition is maintained. This requires the regulation and removal of water, ions and both nutritive and waste products. The parenchyma of the central nervous system is devoid of lymphatic vessels [17], which in other organs, is critical for maintaining tissue homeostasis [18]. The way the brain maintains ISF homeostasis is currently unclear [19]. Iliff et al. [20] propose a glymphatic pathway, whereby cerebrospinal fluid (CSF) enters the brain via the paravascular spaces along the penetrating arteries on the surface of the brain (peri-arterial spaces), subsequently passing through the astroglial end-feet and enters the parenchymal tissue where it mixes with ISF and exits (dragging along waste products such as Aβ) via peri-venous spaces. Interestingly, ageing and activity (such as sleep) are also known to influence the functioning of the glymphatic system [21,22].

The intricate nature of the glymphatic system is further amplified by the complex, and broad spectrum of disorders that constitute dementia. It is therefore important to define novel clinically relevant biomarkers that can capture the underlying transport phenomena of the glymphatic system, whilst also being generic enough in order to be interrogated via large-scale statistical analyses. In this work, the precision medicine workflow allows for the peri-arterial swelling and peri-venous drainage (outputs of the *in silico* model) to be explored for different genders and activity levels, as these components are central to the glymphatic system hypothesis. This approach allows for a previously unexplored understanding of the disease trajectory (from MCI to AD), and extends the approach used to interrogate the NVU in the region of the hippocampus [55]. The central driver of the *in silico* model presented here is a surrogate model that outputs arterial blood flow waveforms that are used as boundary conditions whilst taking into account the otherwise challenging nature of LEFs [26] and subject profiles. In addition, an imaging pipeline is used to further personalise the workflow via the acquisition of a

subject-specific atlas of ISF/CSF permeability within the parenchymal tissue; and also, the accurate representations of the cerebroventricular geometries.

1.2 Aortic Dissection (AoD)

Aortic dissection is an extremely severe vascular condition with high mortality rates. With an incidence of 3-4 cases per 100,000 every year in the United Kingdom and United States, it represents the most common aortic emergency, more frequent than ruptured aneurysms [29].

AoD is characterized by the separation of the layers of the aortic wall: a tear in the intima layer allows the blood to flow within the aortic wall inducing the formation of two flow channels, the true (TL) and false lumen (FL), separated by an intimal flap (IF) [30]. Classification and medical management of AoDs is based on the anatomical location of the dissection: those involving the ascending aorta (Type- A) are more dangerous and are treated surgically as soon as possible [31]. AoDs not involving the ascending aorta are commonly managed with best medical treatment (BMT) in the absence of complications, such as rupture, end-organ malperfusion, refractory pain or hypertension. They include the 'classic' Type-B dissections (involving only the descending thoracic aorta), the 'Arch B' dissections (involving the aortic arch and the descending thoracic aorta) [32] and the 'residual post Type-A' dissections (involving the aortic arch and the descending thoracic aorta after the surgical replacement of the ascending thoracic aorta). However, BMT alone is associated with poor long-term prognosis, with invasive re-intervention in up to 50% of the patients [33]. The identification of patients at risk of developing adverse events at an early stage would allow them to undertake pre-emptive endovascular treatment (TEVAR) in the acute or subacute phase, avoiding the challenges of chronic repair procedures [34].

Management and treatment of AoD are highly patient-specific and morphological features, flow patterns, pressures, velocity and shear rates are extremely important features for this pathology. Hence, patient-specific CFD may lead to objective and quantifiable predictors of adverse outcomes and assist the clinical decision-making around the treatment of Type-B AoDs [35,36].

In a clinical scenario, the datasets used to inform the CFD models are often incomplete and noisy, and practical, ethical and physical reasons prevent the acquisition of complete datasets necessary to construct fully 'patient-specific' models [37]. Hence, adequate modelling assumptions need to be made to 'fill the gaps'. A challenging and important task is the description of the boundary conditions (BSs); state-of-the-art vascular CFD models adopt 3-elements Windkessel models coupled to the outlet boundaries. 3-element Windkessel models are electrical analogues made of three components: a proximal and a distal resistance, and a compliance (see inset in Fig. 2a)[61]. They are commonly employed to describe the pressure-flow relation at the outlets due to the distal vasculature not included in the 3D model [38]. The parameters of the Windkessel models need to be accurately calibrated to represent the specific patient. In the case of AoDs, the task of the modeller is further complicated by the complex geometries and by the compliance and motion of the arterial wall, which can significantly affect the fluid dynamics results [39].

1.3 Outline of the article

This paper briefly describes two consolidated pipelines that were developed within the life-cycle of the VPH-DARE@IT (focused on Alzheimer's Disease) and VPH-CaSE projects (focused on Aortic Dissection). This section commenced by outlining the motivation behind their development, along with a brief introduction to Dementia, Alzheimer's Disease and the glymphatic system. Subsequently, a brief introduction to Aortic Dissection was made, along with its management and treatment, and finally the motivation behind developing the consolidated pipeline. §1 was concluded with a brief introduction to multiple-network poroelastic theory (MPET). The essential breakdown of the methodology behind the full implementation scheme for both pipelines will follow in §2 (highlighting the integrated nature of

the workflows embedded within the VPH-DARE@IT and VPH-CaSE research pipelines), the clinical data collection protocol used to extract the subject-specific data used in both pipelines, and finally the statistical tests used to analyse the MPET results. In §3, results relating to both pipelines are briefly discussed. For the first pipeline (VPH-DARE@IT), MPET simulations are presented (based on one control and one MCI subject) in order to depict the nature of the solution fields that are obtainable at the level of the parenchyma. Subsequently, a Kruskal-Wallis H-test (to determine if there were differences in peri-arterial swelling and peri-venous drainage in the cortical grey matter between the groups considered, during two levels of activity) and Wilcoxon signed-rank test (to determine whether there was no statistically significant median decrease in peri-arterial swelling and peri-venous drainage in the cortical grey matter when subjects lowered their activity level) was conducted for a cohort of 35 subjects. For the second pipeline (VPH-CaSE), two computational templates for AoD interrogation are described: (i) a rigid-wall modelling approach based on non-invasive datasets commonly collected for AoD monitoring, in which the aortic compliance is approximated with a lumped-parameter, and (ii) a moving-wall modelling approach informed by non-invasive but rich multimodal datasets that include non-routine displacement data. The conclusions to the paper are outlined in §4.

2. METHODOLOGY

2.1 Clinical datasets

The subject-specific datasets used in the MPET modelling of this paper were collected as part of the VPH-DARE@IT project (www.vph-dare.eu), and prospective data collection was conducted at the Istituto di Ricovero e Cura a Carattere Scientifico (IRCCS) San Camillo, Lido di Venezia, Italy. This study, including a total of 103 people, was approved by the joint ethics committee of the Health Authority Venice 12 and the IRCCS San Camillo (Protocol number 2014.08), and all participants gave informed consent prior to participation in the study. A cohort of 35 subjects (n = 20 CHC, n = 15 MCI) was picked from the 103 available subjects. This smaller cohort can be stratified into 4 groups, considering males (M) and females (F): CHC_M (n = 8, age 69.4 ± 8.5 years), CHC_F (n = 12, age 72.5 ± 5.7 years), MCI_M (n = 8, age 75.4 ± 5.0 years) and MCI_F (n = 7, age 74.9 ± 8.2 years).

The clinical datasets used for the AoD modelling were collected as part of the EU project VPH-CaSE (www.vph-case.eu) and consisted of 3 patients with chronic AoD, acquired as part of an ethically approved protocol at San Camillo-Forlanini Hospital (Rome, Italy, Prot. n.: 900/CE Lazio 1), and included contrast-enhanced computed tomography (CT) scans, cardiac Doppler ultrasound (US) measurements, non-invasive blood pressure (BP) measurement, and invasive intra-aortic BP measurements. The dataset of a patient with a chronic Type-B AoD was acquired from the Leeds Teaching Hospitals (NHS Health Research Authority, ref: 12/YH/ 0551, Leeds Teaching Hospitals NHS Trust, ref: 788/RADRES/16), and included: non-invasive BP measures, CT scans, high spatial and temporal resolution electrocardiogram-gated cine-imaging sequences (cine-MRI) and through-plane phase-contrast velocity mapping images (PC-MRI).

2.2 Pipeline developed for investigating Alzheimer's Disease

The Alzheimer's Disease pipeline relies on a computational model making use of poroelastic equations describing fluid flow through a porous medium coupled with deformation of the solid matrix [23-25]. These relationships central to the theory relate the total stress, volumetric fluid flux and fluid content to the primary variables of the two-field formulation, namely the solid matrix displacement and scalar pore pressure. The MPET model was used to conduct mechanistic modelling of fluid transport through the brain parenchyma.

For a research workflow promoting precision medicine, it's imperative that the patient's history, lifestyle and environmental factors (LEFs) are also considered. In this work, a workflow was used to garner a more detailed understanding of the underlying reasons for the variability in disease trajectory, by incorporating LEFs, and interrogating the results based on novel biomechanistic biomarkers that are derived within the realm of fluid transport in the brain. The MPET model allows for the simultaneous solution of continuity and momentum conservation equations, in four interconnected fluid compartments, within a deformable solid matrix (the parenchymal tissue)., and can capture the biomechanical behaviour (brain tissue displacement, pore pressure, filtration velocity, swelling and drainage of the fluid for each compartment) of perfused tissue. For a detailed description on the boundary conditions used, the mesh independence study and the parameters used in this study,

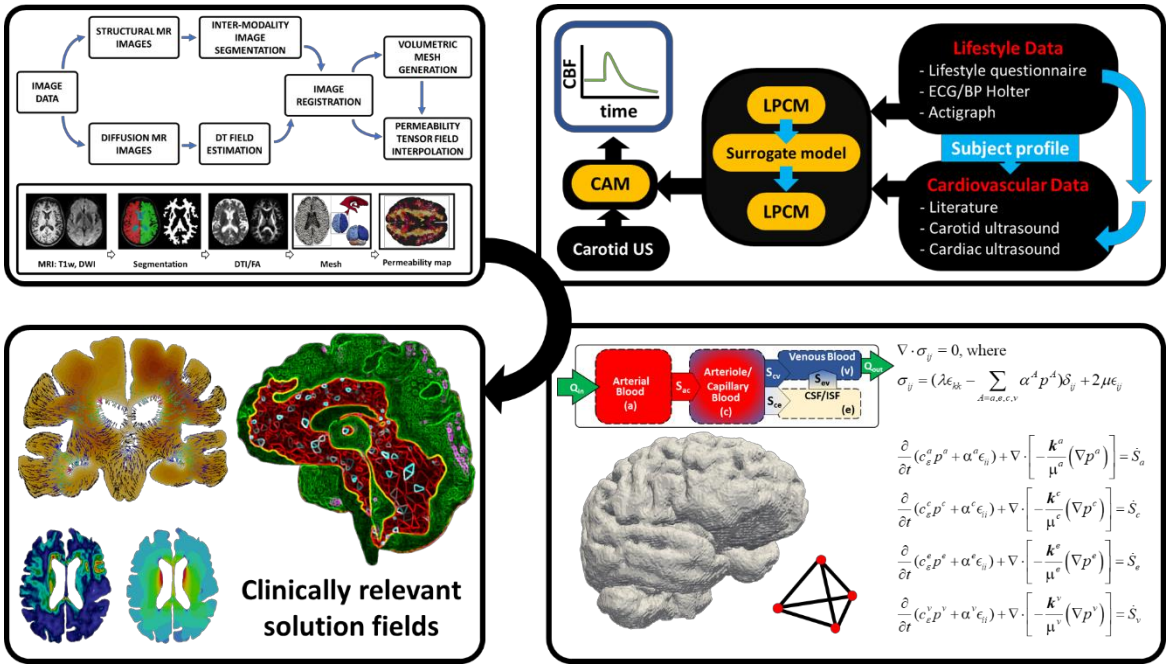

Figure 1. Subject-specific imaging pipeline for acquiring subject-specific cerebroventricular geometries (that are discretised using tetrahedral elements) and permeability tensor maps (top left), personalised cerebral blood flow waveforms (top right) that are fed into the arterial compartment of the MPET solver (bottom right), in the form of a Neumann boundary condition. For the MPET system, the solid matrix represents brain parenchyma, and the communicating fluid phases considered are an arterial network (a), an arteriole/capillary network (c), a CSF/ISF network (mixing the two has been proposed as a candidate for better understanding peri-venous efflux [19] (e) and a venous network (v). A representation of typical solution fields is depicted (bottom left). Ageing and lifestyle related patient-specific boundary conditions are generated following the data collection and subject-based model parameterisation. The personalisation of the lumped parameter circulation model was accelerated via a surrogate model to approximate its input-output response. LPCM = Lumped parameter circulation model, CAM = cerebral autoregulation model.

the reader is referred to work by Vardakis et al. [55] and Guo et al. [28].

The modelling pipeline presented here is personalised for individual subjects on three levels: cerebroventricular geometries (accompanied by the relevant meshes) were extracted from structural MR images; spatial maps of CSF/ISF compartment permeability tensors were estimated from diffusion MR data; and arterial blood flow waveforms, used as cortical surface boundary conditions, were derived from measurements of blood pressure, flow velocity, and other inputs as described in Guo et al [28].

A key component of the subject-specific modelling pipeline (see Figure 1) is the personalised boundary conditions for arterial blood flow. Subject-specific, 24-hour blood flow variability is obtained through a combination of ambulatory blood pressure measurements, clinical ultrasound flow measurements, and mathematical modelling. A lumped parameter circulation model (LPCM) [40] is used to simulate continuous arterial blood flow and translate the spot measurements collected every 15 min during the day and every 30 min during the night, to continuous waveforms of arterial blood flow. Two specific measurements were chosen from the 24-hour recording as indicative of the subject's

activity –high activity (e.g. exercise) identified by highest peak values of arterial blood flow within 24-hours; and low activity (e.g. sleep) identified by the lowest peak values. The waveforms corresponding to these two activity states were used in the subject-specific modelling of this manuscript as boundary conditions for the arterial compartment at the cortical surface (four waveforms were calculated at every time point, which are the ICA blood to the left and right cerebrum, and the vertebral artery blood to the left and right cerebellum). The reader is directed to two relevant publications for further details regarding the personalised boundary conditions and the protocol of their application in the MPET numerical template [28, 40].

Each subject that was analysed had several measurement modalities collected as part of the study, such as: lifestyle questionnaires and neuropsychological tests, whole brain MR imaging, clinical ultrasound flow imaging, portable Holter recordings of blood pressure, and actigraph measured activity levels. Further details can be found in Guo et al. [28]. T1-weighted and diffusion-weighted MR images were processed via a fully automated workflow to create accurate 3D whole-brain meshes and permeability tensor maps (PTMs) of the parenchyma (translating to a heterogeneous and anisotropic permeability field for the CSF/ISF compartment) were extracted using the workflow described in detail in Guo et al. [28]. The consolidated workflow described here, has been embedded within the MULTI-X (www.multi-x.org) cross-domain research platform. Such a platform must address the issues revolving around scalability, reproducibility, flexibility interoperability, fast prototyping, workflow management, data management, data visualisation, licensing and IP management, cost assessment, security and compliance, and importantly, collaboration [41].

2.3 Pipeline developed for investigating Aortic Dissection

For the case of AoD, two different *in silico* explorations were conducted, one, based on the typical datasets available to clinicians, the second, based on a rich, multimodal dataset acquired for research purposes. In the case of the typical, clinically available information, the monitoring of AoD usually involves non-invasive datasets which include contrast-enhanced CT scans, cardiac Doppler US and non-invasive BP measurements. In this section, a CFD framework for personalised rigid-wall simulation informed by commonly available clinical datasets is presented.

Figure 2a shows the pipeline followed for the implementation of the computational model. The AoD geometry is extracted from contrast-enhanced CT scans using semi-automatic thresholding algorithms implemented in the image-processing software Simpleware ScanIP (Synopsys Inc., CA, USA). The stroke volume (SV) and heart rate (HR) of the patient are extracted from cardiac US measurements and are used to personalise a typical flowrate template curve to be used as inflow condition. Model parameters (i.e. Windkessel parameters and aortic compliance) are fine-tuned with a personalisation procedure which combines time-dependent simulations on a reduced-order 0D model and 3D steady-state simulations, as detailed in [49]. The calibration objectives are: (i) to achieve physiological blood flow distribution among the model outlets, and (ii) to obtain the target systolic (P_{sys}) and diastolic (P_{dia}) blood pressures at the inlet, as derived from the non-invasive blood pressure measurements. The fine-tuned parameters are then used in the (geometric) multi-scale CFD model (Figure 2a) in which the fluid-structure interaction effects due to the compliance of the aorta are modelled via a lumped capacitor (C_{aorta}) proximal to the inlet of the 3D model [50]. More advanced patient-specific CFD models that include the motion of the arterial wall require richer multi-modal datasets. This section describes a CFD template that employs a moving-boundary method (MBM) to account for arterial wall compliance and IF motion in CFD simulations (Figure 2b). The model is informed by CT scans, PC-MRI or US flow data, non-invasive BP measurements and by cine-MRI-derived displacement data. The MBM adopts physiologically-supported calculations based on pressure differences and fluid forces in the computational domain along with wall stiffness estimated in different regions of the vessel, as detailed in Bonfanti et al. [48]. Reduced-order 0D models and 3D rigid-wall simulations are used to calibrate the parameters employed in the compliant model, with the same calibration objectives described in the previous section [46].

For both cases, CFD simulations were solved with ANSYS-CFX 18.0 (ANSYS Inc., PA, USA). The Navier-Stokes equations are spatially and temporally discretised with a high-resolution advection scheme and a second order implicit backward Euler scheme [47], respectively, using a uniform time-step of 1 ms, small enough for time-step size-independent results. Further details on the simulation settings can be found in Bonfanti et al. [46].

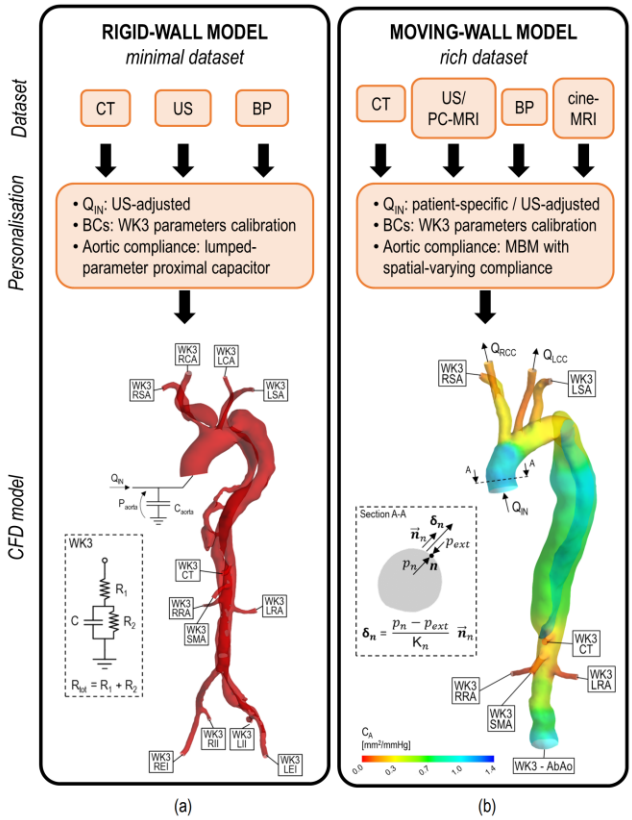

Figure 2: Schematic of the pipelines for the two AoD CFD templates: (a) *Rigid-wall models informed by minimal datasets*, WK3 indicates the Windkessel models coupled at the outlets (see inset) (b) *Moving-wall models informed by rich datasets*, the colour map shows the spatial-varying area compliance of the aorta (C_A = ΔA/ΔP, ΔA: cross-sectional area variation during the cardiac cycle, ΔP: pressure variation during the cardiac cycle), estimated from patient-specific cine-MRI data. The inset shows a cross-section of the ascending aorta and a schematic depicting how the displacement δ of a node *n* on the vessel wall is related to the pressure p_n calculated in the fluid domain and to the stiffness coefficient K_n, according to the moving boundary method (MBM).

3. RESULTS & DISCUSSION

3.1 Alzheimer's Disease

Figure 3 depicts five typical solution fields arising from the MPET solver for two subjects (79-year-old male with MCI and a 73-year-old female cognitively healthy control), namely peri-arterial and peri-venous swelling, peri-arterial and peri-venous drainage, clearance of CSF/ISF, intracranial pressure with overlapping blood velocity vectors. Comparing the results between the control and MCI case, the clearance of CSF/ISF is higher for the control, in addition to it being largely segregated to the periventricular region.

Figures 4a-d depicts the results for peri-arterial and peri-venous swelling and drainage in the cortical grey matter. These results cover the cohort of 35 subjects (and are stratified with respect to gender, disease status and activity level). A Kruskal-Wallis H-test was conducted to determine if there were differences in peri-arterial swelling and peri-venous drainage in the cortical grey matter of the brain between 4 groups (stratified with respect to gender and disease status), during two levels of activity (high and low). A Wilcoxon signed-rank test was used to determine whether there was no statistically significant median decrease in peri-arterial swelling and peri-venous drainage in the cortical grey matter when CHC and MCI subjects lowered their activity level. This is a novel adaptation MPET model. In this example, the focus was on the cortical grey matter. This allows one to interrogate the complex pathophysiology of the brain-wide perivascular system (the "glymphatic system"). Boespflug et al. [42] postulated that the enlarged perivascular space (ePVS) is a possible marker of glymphatic dysfunction in the AD brain. In this work, the assumption that water diffuses between the perivascular spaces and tissue (thereby incorporating the macroscopic effects of aquaporin-4 [43]) [44,45] is

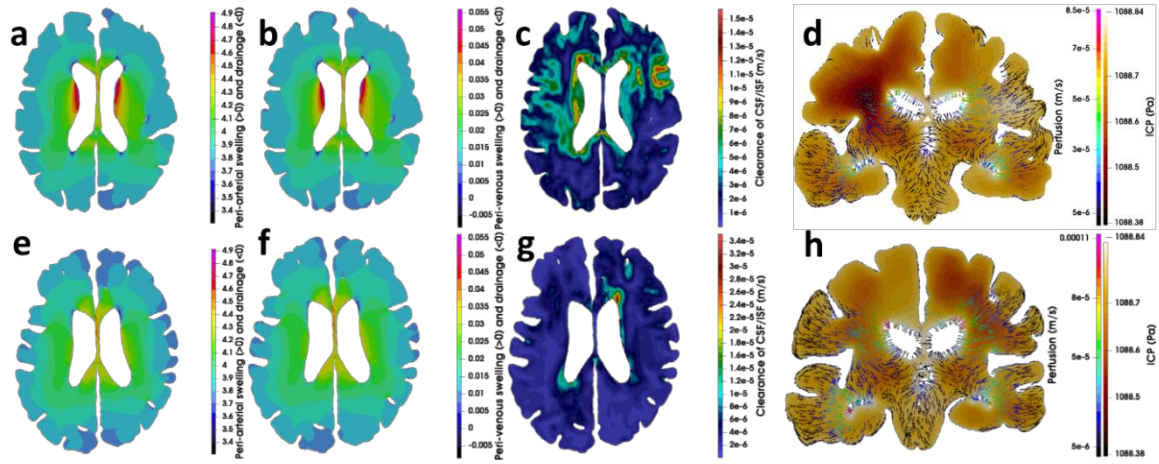

Figure 3. A selection of MPET results (axial and coronal slices) for the brain parenchyma for two subjects, a 79-year-old male with MCI and a 73-year-old female cognitively healthy control. Specifically, results are shown for peri-arterial and peri-venous swelling (positive values of the fluid content of the arterial and venous MPET compartments), peri-arterial and peri-venous drainage (negative values of the fluid content in the same compartments), clearance of CSF/ISF (Darcy velocity of the CSF/ISF compartment), intracranial pressure (pore pressure of the CSF/ISF compartment) with overlapping blood perfusion (Darcy velocity of the capillary compartment) velocity vectors. (a-c) Coronal section of the brain at the level of the lateral ventricles for the MCI subject. (d) An axial slice of the brain (MCI subject), with the intracranial pressure of the parenchyma overlapping with the Darcy velocity vectors of the capillary compartment (perfusion). (e-g) Coronal section of the brain at the level of the cerebral ventricles for the CHC subject. (h) An axial slice of the brain (CHC subject), with the intracranial pressure of the parenchyma overlapping with the perfusion solution field. The magnitude of the velocity vectors has been halved to improve visibility. All results were acquired during a period of high activity.

incorporated, and it is assumed that the ePVS in the cortical grey matter occurs as a direct result of the peri-arterial swelling (the accumulation of fluid in the arterial compartment).

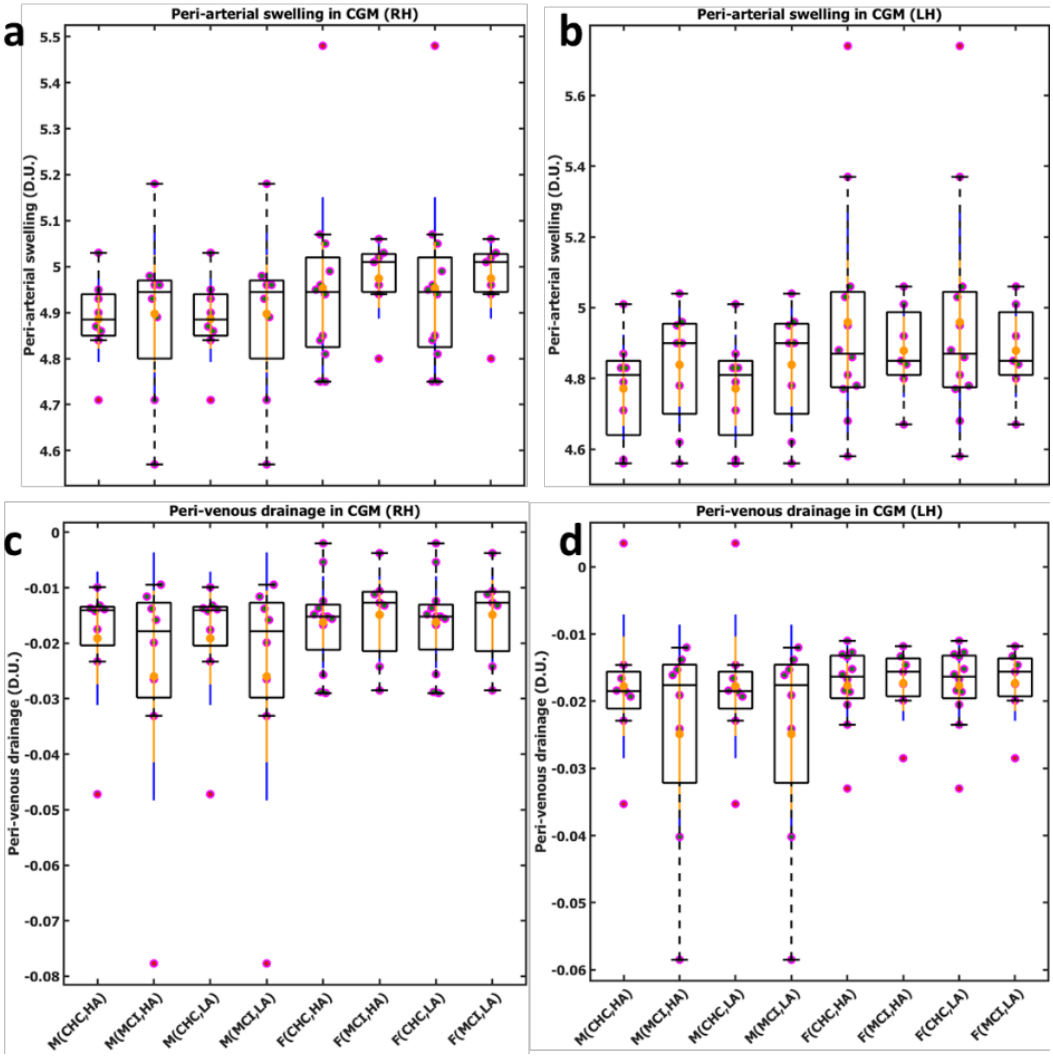

e

	Right Hemisphere				Left Hemisphere			
	HA		LA		HA		LA	
	χ^2	p	χ^2	p	χ^2	p	χ^2	p
CGM_S	4.74	**0.192**	4.74	**0.192**	2.36	0.501	2.44	0.486
CGM_D	5.55	**0.136**	5.55	**0.136**	3.77	0.287	3.77	0.287

Figure 4. Box and whisker plots depict the MPET results for peri-arterial swelling (a, b) and peri-venous drainage (c, d) in left and right hemispheres (LH, RH) for the cohort of 35 subjects. Both sets of results are stratified with respect to males and female groups, with raw data points laid over a 1.96 SEM (95% confidence interval) in orange and a 1 SD in blue. Means are also shown with an orange circle. Raw data is dispersed along the *x*-direction, for clarity. A Wilcoxon Signed Rank Test showed that when comparing the four groups during high and low activity, there were differences in the degree of peri-arterial swelling and peri-venous drainage, but these differences were not statistically significant. (e) Kruskal-Wallis H-Test for peri-arterial swelling and peri-venous drainage in the cortical grey matter. CHC = Cognitively Healthy Control, MCI = Mild Cognitive Impairment, CGM = Cortical Grey Matter, S = swelling, D = drainage, M = male, F = female, HA = High Activity, LA = Low Activity.

It has been suggested that systemic hypertension can cause stiffening and microvascular distortion of vessels, in addition to being associated with reduced capillary density [60]. The trajectory of such a clinically relevant problem can be captured using the personalised modelling pipeline presented in this work. Microvascular permeability and overall cerebral compliance can be linked within the numerical template, thus providing insight (via remodelling processes which account for white matter alterations associated with AD) into the influence of lifestyle and environmental factors, and age-dependent vascular compliance (through a more detailed understanding of cerebral hypoperfusion [28]) [55].

The generic MPET model for perfused parenchymal tissue can be used to provide insight into the underlying mechanisms of the NVU in different regions of the brain on similar-sized subject cohorts [55], to account for aqueductal stenosis during hydrocephalus [43], provide insight into oedema formation within parenchymal tissue [56, 57], offer personalised management of surgical procedures that affect the cerebroventricular system (such as endoscopic third and fourth ventriculostomy) [57, 58] and may also be applied to the study of other organs [59].

3.2 Aortic Dissection pipeline

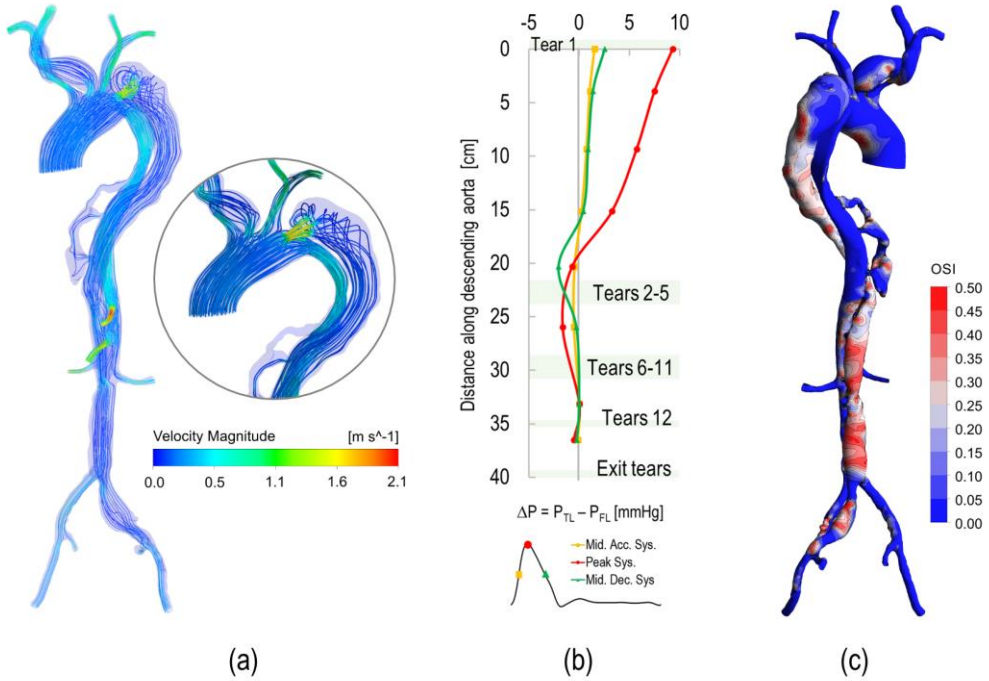

Figure 5: (a) Velocity streamlines at peak systole. High blood velocities, that translate in high wall shear stresses, can be noted at the level of the first entry-tear, whereas vortical flow can be observed in the proximal part of the false lumen (FL). (b) Pressure difference (ΔP) between the true lumen (TL) and the FL calculated at three different phases of the cardiac cycle along the dissection. Negative values of ΔP at the level of the abdominal aortic branches (next to the location of the tears 2-5) may lead to dynamic compression of the TL due to intimal flap (IF) motion and consequently hinder the blood flow in these important branches. (c) Oscillatory shear index (OSI) contour map. High OSI values can be seen in the FL indicating disturbed flow.

The multiscale rigid-wall CFD approach was successfully applied to 3 complex cases of AoDs involving the descending aorta, with datasets acquired at the San Camillo-Forlanini Hospital (Rome, Italy). The proximal lumped-capacitor allowed obtaining reliable blood pressure predictions in the rigid-wall models, as proved by the comparison against patient-specific invasive intra-aortic BP measurements [49]. Haemodynamic results showed how small tears in the distal IF induce disturbed flow in both lumina. Moreover, oscillatory pressures across the IF were often observed in proximity to the tears in the abdominal region, which could indicate a risk of dynamic obstruction of the TL. As an example, Fig. 5 shows some of the results obtained for one of the patients.

The proposed rigid-wall multiscale approach greatly enhances the haemodynamic information available for AoD patients by combining commonly available non-invasive datasets with CFD modelling. However, in certain AoD settings, the rigid-wall approximation does not allow an accurate simulation of the intra-aortic haemodynamics. This is the case of acute AoD settings, in which the IF motion is significant, and of dissections lacking, or with small, re-entry tears [51]. The multiscale compliant approach allows accounting for vessel wall motion effects, as shown in a case-study of a Type-B AoD with dataset provided by the Leeds Teaching Hospitals [46]. The comparison against MRI-derived flow and displacement data (Fig. 6) demonstrated that this approach can accurately represent the aortic haemodynamics overcoming the limitations of rigid-wall approaches.

CFD modelling for AoD can provide valuable insight in the pathology providing information impossible to obtain in vivo in a clinical setting. Such information can be used to predict possible outcomes, such as FL thromboses - correlated to regions of low velocities and oscillatory wall shear stresses (WSS) [52] - or dissection propagation - correlated to areas of elevated WSS [53]. Moreover, intra-luminal blood pressure and its imbalance between the TL and FL could give indication on potential complications, such as FL expansion and TL collapse [54].

The approaches presented in this work can represent the basis to further develop clinical applications of CFD models. For instance, to simulate complex surgical procedures [27] and investigate the best outcome on a patient-specific basis, especially in those vascular pathologies where treatment and management are still a clinical challenge, such as AoD.

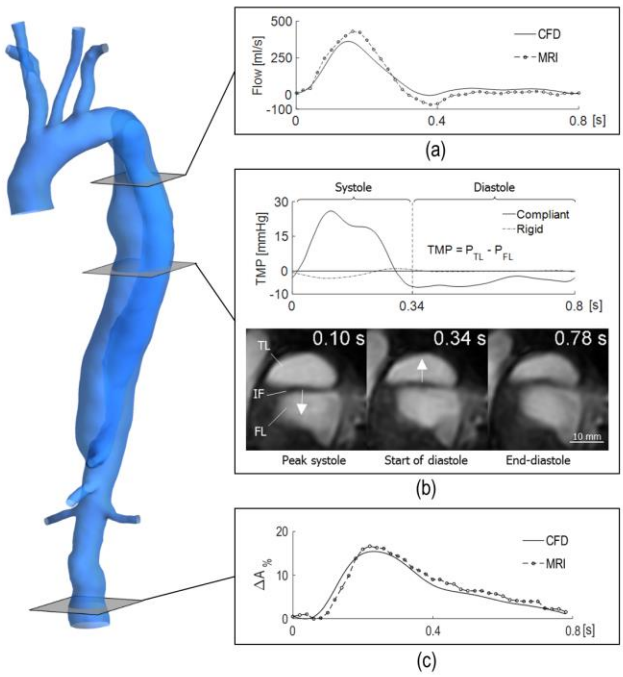

Figure 6: Compliant CFD model results and patient-specific MRI data: (a) Comparison between the flow rate waves in the TL from the CFD model and PC-MRI data. (b) Comparison between the trans-mural pressures (TMP) across the IF obtained with the compliant model (solid line) and the IF displacement observed from 2D cine-MR images at different time instances (TMP = P_{TL} - P_{FL}, where P_{TL} and P_{FL} are the pressures in the TL and FL averaged over a cross-section located at the same level of the 2D cine-MRI slice). It can be noted that the direction of the IF displacement agrees well with the sign of the TMP: a positive TMP corresponds with the motion of the IF through the FL, whereas a negative TMP relates to the motion of the IF through the TL. A rigid model (dashed line) fails to predict the correct TMP. (c) Percentage cross-sectional area variation ($\Delta A_{\%}$) during a cardiac cycle at the level of the abdominal aorta: comparison between CFD results and 2D cine-MRI. $\Delta A_{\%} = (A - A_0)/A_0$, where A is the cross-sectional area of the vessel lumen and A_0 is the lowest cross-sectional area of the vessel lumen throughout a cardiac cycle.

3.3 Lessons learned and commonalities

Both biophysical workflows presented in §2.3 and §2.4 tackle questions in two areas of the human body with unique vascular requirements and underlying pathophysiological cascades. This, however, does not imply disparate requirements for the workflows themselves. Both share the need for highly personalised blood flow boundary conditions (informed by LEFs), and very accurate geometric representations of the volumes that both numerical models (MPET and CFD) ultimately depend upon. Importantly, both workflows can cope with large, complex multi-modal datasets that provide a template to conduct high-throughput data analysis of the resultant numerical solutions. These can then be defined as important clinical biomarkers in the early differential diagnosis and trajectory of AD, and in the understanding of the pathological cascade driving AoD. Both research workflows can be extended and further validated in order to develop and disseminate novel integrative modelling strategies that unravel the complexity of unexplored vascular disorders and help innovate, integrate and better manage complex and stratified subject profiles based on the principles of evidence-based medicine.

4. CONCLUSIONS

This work showcases two successful VPH technologies that were developed in close collaboration with clinicians and meet the requirements of being able to embed themselves in state-of-the-art precision medicine research platforms (such as MULTI-X). These highly integrated in silico centric workflows are well placed in answering clinical quandaries associated within their respective domains (Alzheimer's Disease and Aortic Dissection), in addition to offering perspective clinical solutions (or treatment options) to challenging individual cases through the incorporation of a multitude of personalised data profiles.

The first study was developed through the VPH-DARE@IT project and incorporates a novel three-dimensional multicompartmental poroelasticity model for perfused parenchymal tissue coupled with an automated image-based model personalization workflow, and a subject-specific blood flow variability model. A cohort of 35 subjects was used to test the consolidated pipeline in order to provide insight into the underlying mechanisms of the glymphatic system in the cortical grey matter of the brain, and to ascertain whether physical activity would have an influence in both peri-arterial swelling and peri-venous drainage. The second study was developed through the VPH-CaSE project and combines two sophisticated subject-specific multi-scale flow models that utilise both a rigid-wall model informed by minimal datasets and a moving-wall model informed by rich datasets.

5. ETHICAL APPROVAL

The following ethical protocols have been approved for the Alzheimer's Disease study: This prospective data collection was approved by the joint ethics committee of the Health Authority Venice 12 and the IRCCS San Camillo (Protocol number 2014.08), and all participants gave informed consent prior to participation in the study.

The following ethical protocols have been approved for the aortic dissection study: NHS Health Research Authority, ref: 12/YH/ 0551, Leeds Teaching Hospitals NHS Trust, ref: 788/RADRES/16, A.O. San Camillo Forlanini, Prot. n.: 900/CE Lazio 1. The patients signed the appropriate consent form.

6. ACKNOWLEDGEMENTS

The consolidated pipeline allied to the Alzheimer's Disease study was supported by the European Commission FP7 project VPH-DARE@IT (FP7-ICT-2011-9-601055), and partially by the EPSRC-funded projects OCEAN (EP/M006328/1) and EPSRC-NIHR HTC Partnership Award 'Plus': Medical Image Analysis Network (EP/N026993/1). MB is supported by the European Union's Horizon 2020 research and innovation programme (Marie Sklodowska-Curie GA No. 642612, www.vph-case.eu); MB and VDZ are supported by the Wellcome/EPSRC Centre for Interventional and Surgical Sciences (WEISS) (203145Z/16/Z); VDZ is supported by the Leverhulme Trust (Senior Research Fellowship No. RF-2015-482).

This is a summary of independent research carried out at the National Institute for Health Research (NIHR) Sheffield Biomedical Research Centre (Translational Neuroscience). The views expressed are those of AV and the remaining authors, and not necessarily those of the NIHR or the Department of Health.

REFERENCES

[1] M. Viceconti, E. Dall'Ara. From bed to bench: How in silico medicine can help ageing research. Mechanisms of Ageing and Development, 177 (2019); pp. 103-108

[2] C. Patterson. World Alzheimer's Report 2018. Alzheimer's Disease International, (2018).

[3] J. M. Tublin, J. M. Adelstein, F. del Monte, C. K. Combs, L. E. Wold. Getting to the Heart of Alzheimer's Disease. Circ Res, 124 (2019); pp. 142-149

[4] J. M. Tarasoff-Conway, R. O. Carare, R. S. Osorio, L. Glodzik, T. Butler, E. Fieremanset, et al. Clearance systems in the brain-implications for Alzheimer disease. Nat Rev Neurol, 11(2015); pp. 457–470.

[5] A. Ramanathan, A. R. Nelson, A. P. Sagare, B.V. Zlokovic. Impaired vascular-mediated clearance of brain amyloid beta in Alzheimer's disease: the role, regulation and restoration of LRP1. Front. Aging Neurosci. 7 (2015)

[6] R. F. Gottesman, A. L. Schneider, Y. Zhou, J. Coresh, E. Green, N. Gupta, et al. Association Between Midlife Vascular Risk Factors and Estimated Brain Amyloid Deposition. JAMA, 317(2017); pp. 1443–1450.

[7] A. E. Roher, J. P. Debbins, M. Malek-Ahmadi, K. Chen, J. G. Pipe, S. Maze, et al. Cerebral blood flow in Alzheimer's disease. Vascular health and risk management, 8(2012); pp. 599–611

[8] T. Thomas, S. Miners, S. Love. Post-mortem assessment of hypoperfusion of cerebral cortex in Alzheimer's disease and vascular dementia. Brain, 138(2015); pp. 1059–1069.

[9] J. C. de la Torre. Is Alzheimer's disease a neurodegenerative or a vascular disorder? Data, dogma, and dialectics. Lancet Neurol, 3(2004); pp. 184–190

[10] D. A. Drachman. The amyloid hypothesis, time to move on: amyloid is the downstream result, not cause, of Alzheimer's disease. Alzheimer's Dement, 10 (2014), pp. 372–380

[11] B. P. Austin, V. A. Nair, T. B. Meier, G. Xu, H. A. Rowley, C. M. Carlsson, et al. Effects of hypoperfusion in Alzheimer's disease. J. Alzheimer's Dis, 26 (2011); pp. 123–133

[12] T. Thomas, S. Miners, S. Love. Post-mortem assessment of hypoperfusion of cerebral cortex in Alzheimer's disease and vascular dementia. Brain, 138(2015); pp. 1059–1069

[13] M. Mazza, G. Marano, G. Traversi, P. Bria, S. Mazza. Primary cerebral blood flow deficiency and Alzheimer's disease: shadows and lights. J Alzheimers Dis, 23(2011); pp. 375–89

[14] A. Ruitenberg, T. den Heijer, S. L. Bakker, J. C. van Swieten, P. J. Koudstaal, A. Hofman, et al. Cerebral hypoperfusion and clinical onset of dementia: the Rotterdam Study. Ann Neurol; 57(2005); pp. 789–94

[15] C. Iadecola. Neurovascular regulation in the normal brain and in Alzheimer's disease. Nature Reviews Neuroscience, 5(2004); pp. 347-360

[16] M. Bondi, E. Edmonds, D. Salmon. Alzheimer's Disease: Past, Present, and Future. Journal of the International Neuropsychological Society, 23(2017); pp. 818-831

[17] A. Louveau, B.A. Plog, and S. Antila, K. Alitalo, M. Nedergaard, and J. Kipnis. Understanding the functions and relationships of the glymphatic system and meningeal lymphatics. J Clin Invest, 127 (2017); pp. 3210-3219

[18] S. Da Mesquita, Z. Fu, J. Kipnis. The Meningeal Lymphatic System: A New Player in Neurophysiology. Neuron, 100 (2018); pp. 375-388

[19] E. N. T. P. Bakker, D. M. P. Naessens, E. VanBavel. Paravascular spaces: entry to or exit from the brain?. Exp. Physiol, (2019); pp. 1-5

[20] J.J. Iliff, M. Wang, Y. Liao, B. A. Plogg, W. Peng, G. A. Gundersen, et al. A paravascular pathway facilitates CSF flow through the brain parenchyma and the clearance of interstitial solutes, including amyloid β. Sci Transl Med, 4(2012).

[21] B.T. Kress, J.J. Iliff, M. Xia, M. Wang, H. S. Wei, D. Zeppenfeld, et al. Impairment of paravascular clearance pathways in the aging brain. Ann. Neurol, 76(2014); pp. 845–861

[22] L. Xie, H. Kang, Q. Xu, M. J. Chen, Y. Liao, M. Thiyagarajan, et al. Sleep drives metabolite clearance from the adult brain. Science, 342(2013), pp. 373–377

[23] M. A. Biot. General theory of three-dimensional consolidation. J. Appl. Phys, 12(1941); pp. 155–164.

[24] M. A. Biot. Theory of elasticity and consolidation for a porous anisotropic solid. J. Appl. Phys, 26(1955); pp. 182–185

[25] K. Terzaghi. Principle of soil mechanics. Eng. News Record, A Series of Articles, (1925).

[26] L. Y. Di Marco, A. Marzo, M. Muñoz-Ruiz, M. A. Ikram, M. Kivipelto, D. Ruefenacht, et al. Modifiable lifestyle factors in dementia: a systematic review of longitudinal observational cohort studies. J Alzheimers Dis, 42(1)(2014); pp.119-35

[27] D. Chen, M. Müller-Eschner, D. Kotelis, D. Böckler, Y. Ventikos, H. von Tengg-Kobligk, A longitudinal study of Type-B aortic dissection and endovascular repair scenarios: computational analyses. Medical Engineering & Physics, 35(9)(2013); pp. 1321-1330

[28] L. Guo, J. C. Vardakis, T. Lassila, M. Mitolo, N. Ravikumar, D. Chou, et al. Subject-specific multi-poroelastic model for exploring the risk factors associated with the early stages of Alzheimer's disease. Interface Focus, 8(2018).

[29] S. G. Thrumurthy, A. Karthikesalingam, B. O. Patterson, P. J. E. Holt, M. M. Thompson. The diagnosis and management of aortic dissection. BMJ, 344(2012).

[30] C. A. Nienaber, R. E. Clough, Management of acute aortic dissection. The Lancet, 385 (2015); pp. 800–811

[31] R. Erbel, V. Aboyans, C. Boileau, E. Bossone, R. Di Bartolomeo et al. 2014 ESC Guidelines on the diagnosis and treatment of aortic diseases. Eur Heart J, 35 (2014); pp. 2873–2926.

[32] S. Trimarchi, H. W. L. de Beaufort, J. L. Tolenaar, et al. Acute aortic dissections with entry tear in the arch: A report from the International Registry of Acute Aortic Dissection. J. Thorac. Cardiovasc. Surg., 157(1) (2019), pp. 66–73.

[33] A. V. Kamman, J. Brunkwall, E. L. Verhoeven, R. H. Heijmen, S. Trimarchi. Predictors of aortic growth in uncomplicated type B aortic dissection from the Acute Dissection Stent Grafting or Best Medical Treatment (ADSORB) database. J Vasc Surg; 65(2017); pp. 964-71

[34] A V. Kamman, H. W. L. de Beaufort, G. H. W. van Bogerijen, F. J. H. Nauta, R. H. Heijmen, F. L. Moll, et al. Contemporary Management Strategies for Chronic Type B Aortic Dissections: A Systematic Review. PLoS One, (2016)

[35] H. Xu, Z. Li, H. Dong, Y. Zhang, J. Wei, P. N. Watton, et al. Hemodynamic parameters that may predict false-lumen growth in type-B aortic dissection after endovascular repair: A preliminary study on long-term multiple follow-ups. Med Eng Phys, 7(35)(2017)

[36] H. Xu, M. Piccinelli, B. G. Leshnower, W. R. Taylor, A. Veneziani. Coupled Morphological–Hemodynamic Computational Analysis of Type B Aortic Dissection: A Longitudinal Study. Ann Biomed Eng, (2018).

[37] R. M. Romarowski, A. Lefieux, S. Morganti, A. Veneziani, F. Auricchio. Patient-specific CFD modelling in the thoracic aorta with PC-MRI-based boundary conditions: A least-square three-element Windkessel approach. Int J Numer Method Biomed Eng, 34(2018)

[38] S. Pirola, Z. Cheng, O. A. Jarral, D. P. O'Regan, J. R. Pepper, T. Athanasiou, et al. On the choice of outlet boundary conditions for patient-specific analysis of aortic flow using computational fluid dynamics. J Biomech, 60 (2017).

[39] M. Alimohammadi, J. M. Sherwood, M. Karimpour, O. Agu, S. Balabani, V. Díaz-Zuccarini. Aortic dissection simulation models for clinical support: fluid-structure interaction vs. rigid wall models. Biomed Eng Online, 14(34)(2015)

[40] T. Lassila, L. Y. D. Marco, M. Mitolo, V. Iaia, G. Levedianos, A. Venneri, et al. Screening for Cognitive Impairment by Model-Assisted Cerebral Blood Flow Estimation. IEEE Transactions on Biomedical Engineering, 65(7)(2017); pp. 1654-1661

[41] M. H. de Vila, R. Attar, M. Pereanez, A. F. Frangi. MULTI-X, a State-of-the-Art Cloud-Based Ecosystem for Biomedical Research, 2018 IEEE International Conference on Bioinformatics and Biomedicine (BIBM), Madrid, Spain, 2018, pp. 1726-1733.

[42] E. L. Boespflug, M. J. Simon, E. Leonard, M. Grafe, R. Woltjer, L. C. Silbert, et al. Targeted Assessment of Enlargement of the Perivascular Space in Alzheimer's Disease and Vascular Dementia Subtypes Implicates Astroglial Involvement Specific to Alzheimer's Disease. Journal of Alzheimer's disease, 66(4)(2018); pp. 1587–1597

[43] D. Chou, J. C. Vardakis, L. Guo, B. J. Tully, Y. Ventikos, A fully dynamic multi-compartmental poroelastic system: Application to aqueductal stenosis. Journal of Biomechanics, 49 (11)(2016); pp. 2306-2312

[44] M. Asgari, D. de Zelicourt, V. Kurtcuoglu. How astrocyte networks may contribute to cerebral metabolite clearance. Sci Rep, 5(2015).

[45] V. A. Eidsvaag, H. A. Hansson, K. Heuser, E. A. Nagelhus, P. K. Eide. Cerebral microvascular abnormalities in patients with idiopathic intracranial hypertension. Brain Res, 1686 (2018); pp. 72-82.

[46] M. Bonfanti, S. Balabani, J. P. Greenwood, S. Puppala, S. Homer-Vanniasinkam, V. Díaz-Zuccarini. Computational tools for clinical support: a multi-scale compliant model for haemodynamic simulations in an aortic dissection based on multi-modal imaging data. J R Soc Interface, 14(2017)

[47] ANSYS Inc. CFX-Solver Theory Guide. Release 17. (2016)

[48] M. Bonfanti, S. Balabani, M. Alimohammadi, O. Agu, S. Homer-Vanniasinkam, V. Díaz-Zuccarini. A simplified method to account for wall motion in patient-specific blood flow simulations of aortic dissection: Comparison with fluid-structure interaction. Med Eng Phys, 58(2018); pp.72–79

[49] M. Bonfanti, G. Franzetti, G. Maritati, S. Homer-Vanniasinkam, S. Balabani, V. Díaz-Zuccarini. Patient-specific haemodynamic simulations of complex aortic dissections informed by commonly available clinical datasets. Medical Engineering and Physics (2019), doi: 10.1016/j.medengphy.2019.06.012

[50] S. Pant, B. Fabrèges, J. F. Gerbeau, I. E. Vignon-Clementel. A methodological paradigm for patient-specific multi-scale CFD simulations: from clinical measurements to parameter estimates for individual analysis. Int J Numer Method Biomed Eng, 30 (2014); pp. 1614–48.

[51] E. Soudah, P. Rudenick, M. Bordone, B. Bijnens, D. García-Dorado, A. Evangelista, et al. Validation of numerical flow simulations against in vitro phantom measurements in different type B aortic dissection scenarios. Comput Methods Biomech Biomed Engin,18(2015); pp. 805–815

[52] C. Menichini, Z. Cheng, R. G. J. Gibbs, X. Y. Xu. A computational model for false lumen thrombosis in type B aortic dissection following thoracic endovascular repair. J Biomech,66(2018); pp. 36–43.

[53] A. Osswald, C. Karmonik, J. R. Anderson, F. Rengier, M. Karck, J. EngelkeJ, et al. Elevated Wall Shear Stress in Aortic Type B Dissection May Relate to Retrograde Aortic Type A Dissection: A Computational Fluid Dynamics Pilot Study. Eur J Vasc Endovasc Surg, 54 (2017); pp.324–30.

[54] T. T. Tsai, M. S. Schlicht, K. Khanafer, J. L. Bull, D. T. Valassis, D. M. Williams, et al. Tear size and location impacts false lumen pressure in an ex vivo model of chronic type B aortic dissection. J Vasc Surg, 47 (2008); pp. 844–51.

[55] J. C. Vardakis, L. Guo, T. W. Peach, T. Lassila, M. Mitolo, D. Chou, et al. Fluid-Structure Interaction for Highly Complex, Statistically Defined, Biological Media: Homogenisation and a 3D Multi-Compartmental Poroelastic Model for Brain Biomechanics. J of Fluids and Structures. (2019), doi: 10.1016/j.jfluidstructs.2019.04.008

[56] L. Guo, J. C. Vardakis, D. Chou, Y. Ventikos. A multiple-network poroelastic model for biological systems and application to subject-specific modelling of cerebral fluid transport. International Journal of Engineering Science, *In Review*.

[57] J. C. Vardakis, D. Chou, B. J. Tully, C. C. Hung, T. H. Lee, P. H. Tsui. Investigating cerebral oedema using poroelasticity. Medical Engineering and Physics, 38(1)(2016); pp. 48-57

[58] J. C. Vardakis, B. J. Tully, Y. Ventikos. Exploring the Efficacy of Endoscopic Ventriculostomy for Hydrocephalus Treatment via a Multicompartmental Poroelastic Model of CSF Transport: A Computational Perspective. PLoS ONE, 8 (12)(2013)

[59] T. B. Thompson, B. M. Riviere, M. G. Knepley. An implicit discontinuous Galerkin method for modeling acute edema and resuscitation in the small intestine. Mathematical Medicine and Biology: A Journal of the IMA, (2019)

[60] C. Iadecola. The pathobiology of vascular dementia. Neuron, 80(4)(2013); pp. 844-866.

[61] N. Westerhof, J. W. Lankhaar, & B. E. Westerhof. The arterial Windkessel. Med Biol Eng Comput, 47(2)(2009); pp. 131-141.